01,10,12

Study of the FCC-BCC phase transition in an Au-Fe alloy

© M.N. Magomedov

Institute for geothermal problems and renewable energy — branch of the joint Institute of high temperatures
of the Russian Academy problems of Sciences,
Makcachkala, Russia

E-mail: mahmag4@mail.ru

The properties of the disordered Au-Fe substitution alloy are studied based on the analytical method, which uses the paired interatomic potential of Mie–Lennard-Jones. The parameters of the interatomic potential for the FCC and BCC structures of Au and Fe are determined. Based on these parameters, the concentration dependences of the properties of the FCC and BCC structures of the Au-Fe alloy are calculated. Under normal conditions (i.e., pressure $P = 0$ and temperature $T = 300\,\text{K}$), changes in the properties of the Au-Fe alloy at the structural phase transition of FCC-BCC are calculated. Using the RP-model of the nanocrystal, the displacement of the C_f concentration, at which the FCC-BCC phase transition occurs, due to a decrease in the size of the nanoparticle was calculated. It is shown that at an isochoric-isothermal decrease in the number of atoms (N) in an Au-Fe nanoparticle, the C_f value displace towards higher Fe concentrations. For a nanoparticle with a fixed number of atoms and a constant surface shape, the C_f value increases at an isochoric increase in temperature, and the C_f value decreases at an isothermal decrease in density. Calculations have shown that at $N < 59900$ for the $\text{Au}_{1-C}\text{Fe}_C$ alloy at $P = 0$, $T \leq 300\,\text{K}$ and at any iron concentration, the FCC structure is more stable than the BCC structure.

Keywords: gold, iron, substitution alloy, phase transition, state equation, elastic modulus, thermal expansion, nanoparticle, surface energy.

DOI: 10.21883/PSS.2022.13.52307.145

1. Introduction

As was demonstrated in [1–5], substitution solid solution $\text{Au}_{1-C}\text{Fe}_C$, where C is the atomic concentration of iron, forms two stable crystal structures at low temperatures ($T < 600\,\text{K}$) and pressures ($P \approx 0$):

at $0 < C < 68\%$, a Cu-type face-centered cubic (FCC, Fm3m) structure is stable;

at $68 < C < 100\%$, a mixture of body-centered cubic (BCC, Im3m) structures of the α-Fe and δ-Fe type is stable.

However, the changes in thermodynamic properties of this alloy occurring in the structural FCC-BCC phase transition have not been examined experimentally. This is attributable to the fact that the metastable amorphous structure manifests itself in experiments in the $\text{Au}_{1-C}\text{Fe}_C$ alloy at $45 < C < 90\%$ [1,2,4], thus making it difficult to study the „pristine" FCC-BCC transition. In view of this, the boundary of stability of FCC and BCC phases (i.e., C_f) for the Au-Fe alloy is determined only tentatively, and various estimates of C_f have been published. Therefore, no experimental data on changes in the thermodynamic properties of the Au-Fe alloy occurring in the FCC-BCC transition are available in literature even for normal conditions (i.e., $P \approx 0$ and $T = 300\,\text{K}$).

Theoretical studies of the FCC-BCC transition in the Au-Fe alloy are made difficult by the fact that pure gold does not form a BCC structure and iron at $P \approx 0$ has a FCC structure (γ-phase, austenite) only at high temperatures ($T > 1185\,\text{K}$). This gives rise to ambiguity in the

determination of parameters of the interatomic interaction for these phases of pure metals and hinders the theoretical study of the FCC-BCC transition in their substitution alloy.

We have examined the properties of substitution solid solution $\text{Au}_{1-C}\text{Fe}_C$ with the FCC structure in [6] via analytical calculations. In the present study, the mathematical method from [6] is used to study the properties of this alloy both in the BCC phase and in the FCC-BCC phase transition. It is demonstrated that iron is central to this phase transition. The emergence of the metastable amorphous phase in the region of phase transition is explained. In addition, the analytical RP model of a nanocrystal from [6,7] was used to examine changes in the parameters of the FCC-BCC transition induced by a reduction in the size of nanoparticles of the Au-Fe alloy.

2. Study of the properties of Au and Fe crystals in the FCC and BCC phases

In order to calculate the lattice properties of a single-component crystal, we present the pairwise interatomic interaction in the form of the Mie–Lennard-Jones potential [8]:

$$\varphi(r) = \frac{D}{(b-a)}\left[a\left(\frac{r_o}{r}\right)^b - b\left(\frac{r_o}{r}\right)^a\right], \qquad (1)$$

where D and r_o are the depth and the coordinate of the potential minimum and $b > a > 1$ are numerical parameters.

The parameters of interatomic potential (1) for Au (atomic mass $m = 196.967$ a.m.u.) and Fe ($m = 55.847$ a.m.u.) should be determined prior to applying the method from [6] in calculations of the properties of the Au-Fe binary alloy. In addition, one needs to determine the parameters of interatomic potential (1) for Au and Fe with both FCC (where the first coordination number and the packing coefficient are $k_n(\infty) = 12$ and $k_p = 0.7405$) and BCC ($k_n(\infty) = 8$ and $k_p = 0.6802$) crystal structures in order to calculate the properties of the Au-Fe alloy in FCC and BCC phases. For different crystal structures of pure metal, the parameters of the potential of the pairwise interatomic interaction will be different. This is attributable to the redistribution of the electron density over pairwise interatomic bonds that occurs when the crystal structure changes [9].

The parameters of potential (1) for FCC Au were determined in [10,11] and used in [6] to calculate the properties of the FCC Au-Fe alloy. The parameters of potential (1) for FCC Fe were determined in [9] in the study of the FCC-BCC phase transition in iron. The parameters of potential (1) for a mixture of BCC α-Fe and δ-Fe structures were determined and tested in [12].

Since Au does not form a BCC structure under normal conditions [13], the parameters of potential (1) for this modification of gold were estimated in the following way. The empirical relation between the interatomic distance and the packing index of a crystal with a cubic structure was used to determine r_o. While packing index k_p in the course of polymorphic transformations increases in the following sequence [14, p. 288]:

$$k_p = 0.3401 \,(\text{A4} = \text{diamond}) \rightarrow 0.5236 \,(\text{A5} = \text{scp})$$

$$\rightarrow 0.6802 \,(\text{A2} = \text{BCC}) \rightarrow 0.7405 \,(\text{A1} = \text{fcc}),$$

the interatomic bond length increases in the sequence

$$1.02 \rightarrow 1.09 \rightarrow 1.11 \rightarrow 1.14.$$

Thus, the distance between the centers of the nearest-neighbor atoms in transition from the FCC structure to BCC may be estimated using the following relation: $r_o(\text{fcc})/r_o(\text{BCC}) = 1.14/1.11 = 1.027$. Since $r_o(\text{fcc})/[10^{10}\,\text{m}] = 2.8751$ for FCC Au [6,10,11], we find the following for BCC Au: $r_o(\text{BCC}) = 2.7994\,[10^{-10}\,\text{m}]$.

The power parameters of potential (1) for BCC Au were taken equal to those for FCC Au. Potential depth D (bcc-Au) was determined by fitting to the point of intersection of specific (per atom) thermodynamic potentials at $T = 10\,\text{K}$ and $R = 1$ for the FCC and BCC phases of the Au$_{1-C}$Fe$_C$ alloy with iron concentration $C_f = 0.68$. Here, $R = r_o/c$ is the relative linear density of the crystal, $c = (6k_p v/\pi)^{1/3}$ is the distance between the centers of the nearest-neighbor atoms, $v = V/N$ is the specific volume, and V and N are the volume and the number of atoms in the crystal. The obtained intersection of the thermodynamic potentials is shown in Fig. 1, where k_B is the Boltzmann constant.
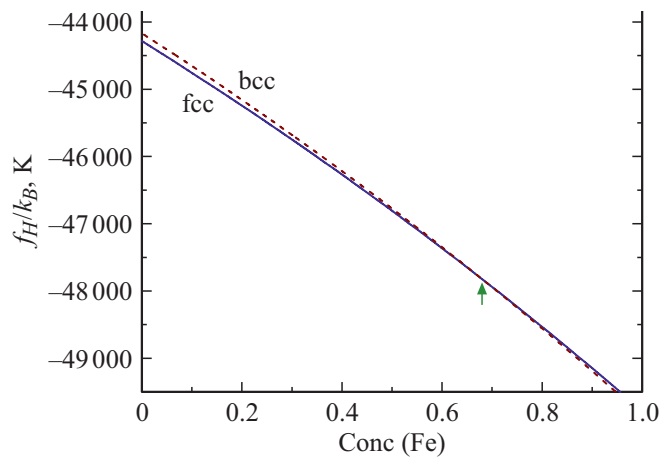
Figure 1. Concentration dependences of the specific thermodynamic potentials for the FCC (solid curve) and BCC (dashed curve) structures of the Au-Fe alloy at $T = 10\,\text{K}$ and $R = 1$. Intersection of the thermodynamic potentials for the FCC and BCC phases at $C_f = 0.68$ is indicated with an arrow (at $D(\text{bcc-Au})/k_B = 11101\,\text{K}$).

The „average atom" method [6,15,16] was used to calculate four parameters of potential (1) for the binary AB-type alloy. Substitution solid solution A$_{1-C}$B$_C$ with N_A and N_B atoms with different atomic masses m_A and m_B is modeled in this method by an isostructural virtual crystal with $N = N_A + N_B$ identical „average" atoms. Mass $m(C)$ of the „average" atom of this virtual material depends on the solution concentration ($C = N_B/N$) and is calculated as the harmonic mean of the masses of atoms constituting the alloy:

$$m(C) = \left(\frac{P_A}{m_A} + \frac{P_B}{m_B}\right)^{-1}. \tag{2}$$

Functions P_A and $P_B = 1 - P_A$ found in Eq. (2) are the geometric probabilities of finding atoms A and B in the substitution solid solution. They are defined as the probabilities that a random point placed on a line with a length of $(1-C)r_{oA} + Cr_{oB}$ ends up within sections r_{oA} and r_{oB}, respectively:

$$P_A(C) = \frac{(1-C)r_{oA}}{(1-C)r_{oA} + Cr_{oB}},$$

$$P_B(C) = \frac{(1-C)r_{oB}}{(1-C)r_{oA} + Cr_{oB}}. \tag{3}$$

The following expression was obtained for the average value of any one of the four H parameters of pairwise interatomic Mie–Lennard-Jones potential (1) of alloy AB [15,16]:

$$H(\text{A}_{1-C}\text{B}_C) = P_A^2 H_A + P_B^2 H_B + 2P_A P_B H_{AB}, \tag{4}$$

where H_{AB} is the parameter of interatomic potential (1) for a lattice in which the probabilities of finding atoms are the same for both atom types ($P_i = 0.5$) with the relaxation of

this lattice to the thermodynamic potential minimum taken into account [15]:

$$r_{oAB} = \left(\frac{r_{oA}^3 + C_N r_{oB}^3}{1 + C_N} \right)^{1/3}, \quad D_{AB} = (D_A D_B)^{1/2},$$

$$b_{AB} = (b_A + b_B)/2, \quad a_{AB} = (a_A + a_B)/2. \quad (5)$$

Here, parameter C_N, which reflects the difference in compression moduli B_i of crystals of pure components for the mixed lattice in which atoms of both types are found with the same probability, takes the form

$$C_N = \frac{B_B}{B_A} \left(\frac{v_{oA}}{v_{oB}} \right) = \frac{B_B}{B_A} \left(\frac{r_{oA}}{r_{oB}} \right)^3. \quad (6)$$

Thus, mass (2) of the „average" atom in the „average atom" method and the parameters of the potential from Eqs. (4) and (5) depend on concentration C and the parameters of potential (1) for pure single-component crystals. This method was used successfully to calculate the properties of substitution solid solutions FCC-Au-Fe in [6] and Si-Ge in [15,16].

In the present case, since experimental data on the elastic modulus of BCC Au are lacking, parameter C_N from Eq. (6) for all Au and Fe phases was derived from the relation that follows from the formula for the elastic modulus at $P = 0$, $T = 0$ K, and $R = 1$:

$$C_N = \frac{B_B}{B_A} \frac{v_A}{v_B} \cong \frac{(k_n Dab)_B}{(k_n Dab)_A} \left(\frac{v_{oA}}{v_{oB}} \right)^2 = \frac{(Dab)_B}{(Dab)_A} \left(\frac{r_{oA}}{r_{oB}} \right)^6. \quad (7)$$

Thus, the FCC-BCC phase transition in the Au-Fe alloy was modeled using the parameters of the pairwise interatomic Mie–Lennard-Jones interaction potential listed in Table 1.

The lattice parameter (l) is related to the distance between the centers of the nearest-neighbor atoms in the following way: $l(\text{fcc}) = 2^{1/2} r_o(\text{fcc})$ and $l(\text{BCC}) = (2/3^{1/2}) r_o(\text{BCC})$. Using the data from Table 1, we find

$$l(\text{fcc-Au}) = 4.0660, \quad l(\text{fcc-Fe}) = 3.5927 \, [10^{-10} \, \text{m}],$$

$$l(\text{bcc-Au}) = 3.2325, \quad l(\text{bcc-Fe}) = 2.8608 \, [10^{-10} \, \text{m}].$$

These values of the lattice parameter agree well with the values determined theoretically for the FCC and BCC phases of Au and Fe in [17, Fig. 1]:

$$l(\text{fcc-Au}) = 4.1\text{-}4.2, \quad l(\text{fcc-Fe}) = 3.42 - 3.50 \, [10^{-10} \, \text{m}],$$

$$l(\text{bcc-Au}) = 3.25\text{-}3.32, \quad l(\text{bcc-Fe}) = 2.79\text{-}2.85 \, [10^{-10} \, \text{m}].$$

In addition, our values of l agree better with the experimental data for FCC Au and the FCC and BCC phases of Fe from [1]:

$$l(\text{fcc-Au}) = 4.0784, \quad l(\text{fcc-Fe}) = 3.6468,$$

$$l(\text{bcc-Fe}) = 2.8665 \, [10^{-10} \, \text{m}].$$

Table 1. Parameters of pairwise interatomic Mie–Lennard-Jones interaction potential (1) for the FCC and BCC phases of Au and Fe

Crystal	r_o, 10^{-10} m	D/k_B K	b	a	Reference
fcc-Au	2.8751	74-19.160	16.05	2.80	[6,10,11]
bcc-Au	2.7994	11101.0	–"–	–"–	
fcc-γ-Fe	2.5404	8374.353	8.37	3.09	[9]
bcc-α-Fe	2.4775	12576.70	8.26	2.95	[12]

The results of calculations performed using the „average atom" method [6,7] revealed that the point of intersection between the thermodynamic potentials of the FCC and BCC phases of $\text{Au}_{1-C}\text{Fe}_C$ shifts slightly toward higher iron concentrations with isobaric ($P = 0$) increase in temperature. The following was obtained at $T = 300$ K: $C_f = 0.684$ at $R = 1$ and $C_f = 0.683$ at $R = 0.9958$ (this corresponds to $P = 0$).

Table 2 presents the properties of macrocrystals of Au and Fe in the FCC and BCC phases at $T = 300$ K and $P = 0$ calculated using the parameters of potential (1) from Table 1. The following notation is introduced in Table 2: $\alpha_p = (\partial \ln V / \partial T)_P$ is the isobaric volumetric coefficient of thermal expansion, C_v and $C_p = C_v(1 + \gamma \alpha_p T)$ are the isochoric and isobaric heat capacities, s is the specific (per atom) crystal entropy, μ_p is the Poisson's ratio, σ is the specific (per unit area) surface energy of face (100) of the crystal, $\sigma'(T)_v$ and $\sigma'(T)_P$ are the isochoric and isobaric temperature derivatives of function σ, and Δ_p is the isothermal logarithmic area (or density) derivative of function σ.

To put this in context, we present experimental data on the properties of FCC Au, FCC Fe, and BCC Fe crystals taken from literature:
for FCC Au:
  $\Theta/[\text{K}] = 165 - 170$ [18], 162.4 ± 2 [19];
  $\gamma = 2.95 - 3.215$ [18];
  $B_T/[\text{GPa}] = 167.5 - 180.5$ [18];
  $B'(P) = 9.58 \pm 0.08$ [18];
  $\alpha_p/[10^{-6} \, \text{K}^{-1}] = 42 - 42.8$ [18];
  $\sigma(100)/[10^{-3} \, \text{J/m}^2] = 1175 - 1850$ [20], 1510 ± 160 [21];
  $\mu_p = 0.42$ [22];
for FCC-γ-Fe (austenite, at $T > 1200$ K):
  $\Theta/[\text{K}] = 222.5$ [23], 250 [24]; $\gamma = 2.203$ [23], 2.0 [24];
  $B_T/[\text{GPa}] = 146.2$ [23], 140 [24], 88.9 ± 5.1 [25];
  $B'(P) = 4.67$ [23], 8 [24], 8.9 ± 0.7 [25];
  $\sigma(100)/[10^{-3} \, \text{J/m}^2] = 1950 - 2500$ [20], (2265) [26];
for bcc-α-Fe (ferrite):
  $\Theta/[\text{K}] = 472.7 \pm 6$ [19], 303.0 [23], 300 [24];
  $\gamma = 1.736$ [23], 1.55 [24];
  $B_T/[\text{GPa}] = 164.0$ [23], 170 [24];
  $B'(P) = 5.50$ [23], 6.2 [24];
  $\alpha_p/[10^{-6} \, \text{K}^{-1}] = 33 - 39$ [27];
  $\sigma(100)/[10^{-3} \, \text{J/m}^2] = 2360$, $(2179\text{-}2463)$ [26], $2400 - 2500$ [28];
  $\mu_p = 0.32$ [29;30, p. 313].

Table 2. Calculated properties of the FCC and BCC phases of Au and Fe at $P = 0$ and $T = 300\,\mathrm{K}$

Property [unit of measurement]	fcc-Au	bcc-Au	fcc-Fe	bcc-Fe
$R = r_{\mathrm{o}}/c$ — relative linear density	0.995699	0.995699	0.996036	0.995857
$V = [\pi N/(6k_p)]c^3$ [cm^3/mol]	10.252	10.302	7.0649	7.1378
c [10^{-10} m]	2.8875	2.8115	2.5505	2.4878
l — lattice parameter [10^{-10} m]	4.0835	3.2464	3.6069	2.8727
Θ — Debye temperature [K]	198.043	203.130	404.941	399.514
$\gamma = -(\partial \ln \Theta/\partial \ln V)_T$ — Gruneisen parameter	3.0008	3.0006	1.7205	1.7023
$q \cdot 10^3 = [(\partial \ln \gamma/\partial \ln V)_T] \cdot 10^3$	7.5662	7.7811	7.9065	7.7075
$z = -(\partial \ln q/\partial \ln V)_T$	3.0158	3.0161	1.7361	1.7176
$B_T = -\nu(\partial P/\partial \nu)_T$ — elastic modulus [GPa]	166.379	165.176	162.835	151.885
$B'(P) = (\partial B_T/\partial P)_T^{1)}$	8.3501	8.3496	5.8534	5.7695
$\alpha_p = \gamma C_v/(B_T V)$ [$10^{-6}\,\mathrm{K}^{-1}$]	42.997	43.050	34.275	36.068
$\alpha_p \cdot B_T = (\partial P/\partial T)_v = (\partial s/\partial \nu)_T$ [10^{-3} GPa/K]	7.1539	7.1109	5.5811	5.47811
$C_v/(Nk_B)$ — isochoric heat capacity	2.9395	2.9364	2.7564	2.7626
$C_p/(Nk_B) = [C_v/(Nk_B)](1 + \gamma \alpha_p T)$	3.0532	3.0501	2.8052	2.8135
s/k_B — normalized specific entropy	5.1394	5.0649	3.0881	3.1253
$\Theta'(P) = (\partial \Theta/\partial P)_T$ [K/GPa]$^{1)}$	3.5708	3.6895	4.2767	4.4782
$C_v'(P)/(Nk_B)$ [10^{-3}/GPa]$^{1)}$	-2.1343	-2.2947	-4.8746	-5.0693
$\alpha_p'(P) = (\partial \alpha_p/\partial P)_T$ [10^{-6}/(K·GPa)]$^{1)}$	-1.9318	-1.9500	-1.0836	-1.2001
$C_p'(P)/(Nk_B)$ [10^{-3}/GPa]$^{1)}$	-7.3343	-7.5425	-6.5048	-6.8582
$\sigma(100)$ — surface energy [10^{-3} J/m^2]	1531.38	1522.54	2217.38	2204.98
$X_{sc} \cdot 10^3 = 10^3 \cdot \sigma(100)/(c \cdot B_T)$	31.8757	32.7856	53.3909	58.3544
μ_p — Poisson's ratio	0.4274	0.4294	0.3682	0.3768
$\sigma'(T)_v = (\partial \sigma/\partial T)_v$ [10^{-6} J/(m^{2}K)]	-50.979	-50.756	-61.147	-60.870
$\sigma'(T)_P = (\partial \sigma/\partial T)_P$ [10^{-6} J/(m^{2}K)]	-98.927	-98.482	-114.194	-116.345
$\sigma'(P)_T = (\partial \sigma/\partial P)_T$ [10^{-3} J/(m^{2}GPa)]$^{1)}$	6.6997	6.7086	9.5022	10.1238
$\Delta_p = -(\partial \ln \sigma/\partial \ln \Sigma)_T = -0.5(\partial \ln \sigma/\partial \ln c)_T$	1.09228	1.09219	1.04699	1.04632

N o t e. $^{1)}$ Calculated by differentiating the parameter numerically with respect to pressure along the isothermal dependence.

It can be seen that the results from Table 2 agree fairly well with the experimental data. Note that our results agree better with the experimental data than the results obtained in [17, Table 1; 22, Table II] with the use of various computer models.

3. Variation of the properties of the Au-Fe alloy in the FCC-BCC phase transition

The properties of the Au-Fe alloy were calculated using the „average atom" method from [6,15,16] and the parameters of the pairwise potential from Table 1. Figures 2−7 present the isochoric-isothermal ($R = r_{\mathrm{o}}/c = 1$, $T = 300\,\mathrm{K}$) concentration dependences of the properties of substitution solid solution $\mathrm{Au}_{1-C}\mathrm{Fe}_C$ for FCC (solid curves) and BCC (dashed curves) structures. Dots connected by thin solid lines in Figs. 2, 3, and 7 denote the results of calculations [22] for the FCC Au-Fe alloy performed using the density functional theory. Dashed straight lines represent the linear dependences of the arithmetic mean over the Fe concentration of the calculated properties of pure Au and Fe crystals.

It can be seen from Figs. 2−7 that the concentration dependences of the studied properties are nonlinear. De-

pendences $\Theta(C)$ and $C_p(C)$ for the FCC and BCC phases intersect at the following points:

$$\Theta(C = 0.723) = 357.37\,\mathrm{K}$$

and $C_p(C = 0.61)/(Nk_B) = 2.897.$

The calculations revealed that the thermodynamic potentials of the FCC and BCC phases of substitution solid solution $\mathrm{Au}_{1-C}\mathrm{Fe}_C$ at $T = 300\,\mathrm{K}$ and $P = 0$ intersect at $C_f = 0.683$. At this concentration, the mass of the „average atom" and the parameters of potential (1) for the FCC and BCC structures of the Au-Fe alloy assume the values listed in Table 3. The difference in masses of the „average atom" for the FCC and BCC structures is attributable to the fact that the geometric probabilities of finding an Au or Fe atom

Table 3. Values of the mass of the „average" atom and the parameters of pairwise interatomic interaction potential (1) for $\mathrm{Au}_{1-C}\mathrm{Fe}_C$ at $C_f = 0.683$ in the FCC and BCC phases

Crystal	m, a.m.u.	r_{o}, 10^{-10} m	D/k_B, K	b	a
fcc-Au-Fe	74.3614	2.64963	8035.86	11.0389	2.9892
bcc-Au-Fe	74.3355	2.58475	12053.99	10.9643	2.8979

in the substitution solid solution are used in the process of averaging in (2).

The parameters from Table 3 and the method from [6] were used to calculate the properties of the FCC and BCC phases of the $Au_{1-C}Fe_C$ solid solution at $C_f = 0.683$, $T = 300\,K$, and $P = 0$. Table 4 lists the obtained values and their relative variation (in %): $\Delta X = [X(BCC) - X(fcc)]/X(fcc)$.

It can be seen from Table 4 that R, Θ, γ, z, $B'(P)$, C_v, C_p, s, $\sigma\,100$), $\sigma'(T)_v$, $\sigma'(T)_P$, and Δ_p remain almost unchanged
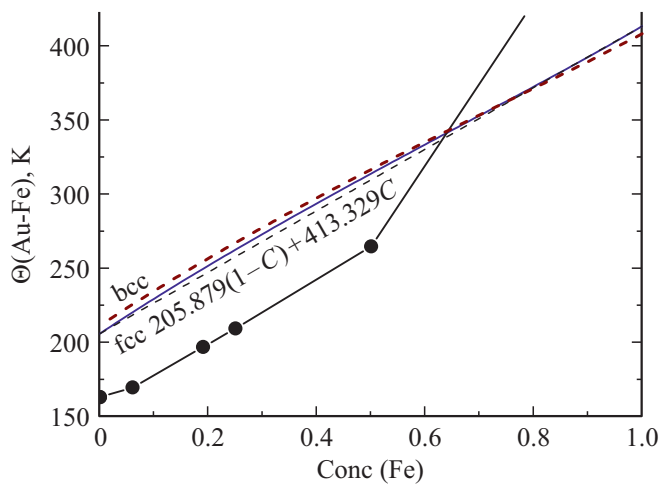
Figure 2. Concentration dependences of the Debye temperature for the FCC (solid curve) and BCC (dashed curve) structures of the Au-Fe alloy. Dots denote the results from [22] for FCC Au-Fe. The dashed straight line represents the linear dependence of the arithmetic mean over the Fe concentration of the Debye temperatures of pure FCC Au and Fe crystals. The dependences for the FCC and BCC structures intersect at $C = 0.723$ and $\Theta = 357.37\,K$.
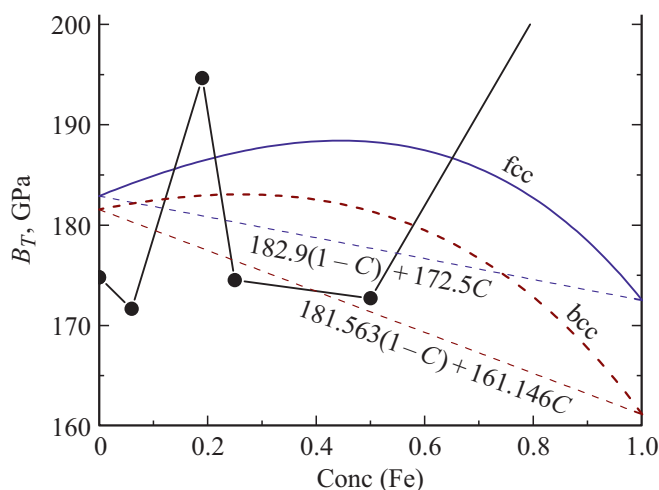
Figure 3. Concentration dependences of the elastic modulus for the FCC (solid curve) and BCC (dashed curve) structures of the Au-Fe alloy. Dots denote the results from [22] for FCC Au-Fe. Dashed straight lines represent the linear dependences of the arithmetic mean over the Fe concentration of the elastic moduli of pure FCC and BCC Au and Fe crystals.
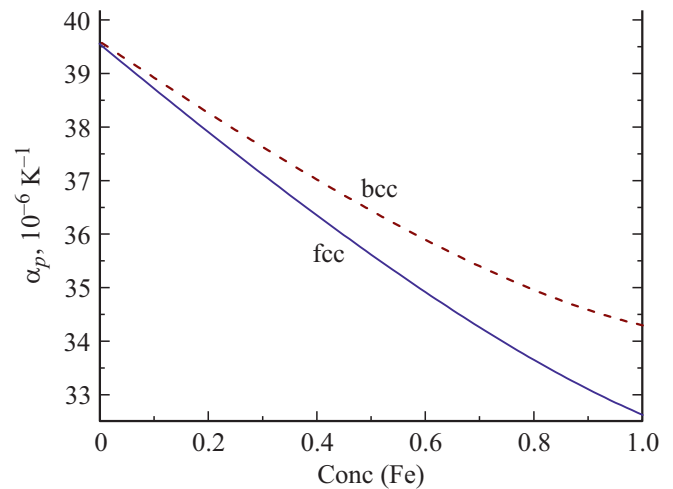
Figure 4. Concentration dependences of the coefficient of thermal expansion for the FCC (solid curve) and BCC (dashed curve) structures of the Au-Fe alloy at $R = 1$ and $T = 300\,K$.
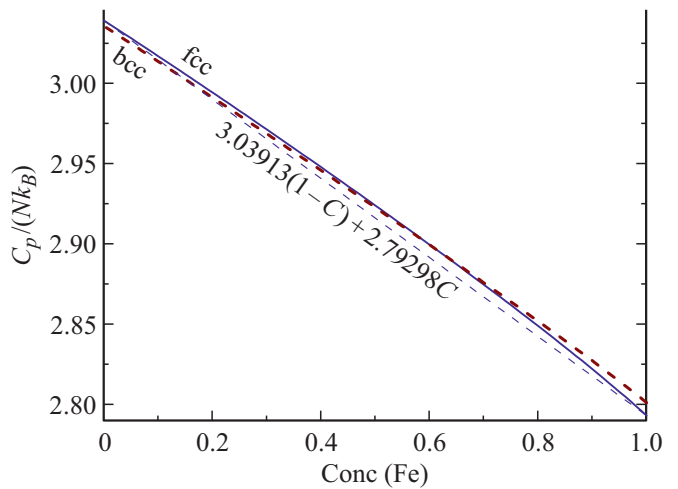
Figure 5. Concentration dependences of the normalized isobaric heat capacity for the FCC (solid curve) and BCC (dashed curve) structures of the Au-Fe alloy. The dashed straight line represents the linear dependence of the arithmetic mean over the Fe concentration of the normalized isobaric heat capacities of pure FCC Au and Fe crystals. The dependences for the FCC and BCC structures intersect at $C = 0.61$ and $C_p/(Nk_B) = 2.897$.

in the process of the FCC-BCC transition in the Au-Fe alloy at $P = 0$ and $T = 300\,K$. The other examined properties vary within $1-7.6\%$, while the lattice parameter undergoes the greatest change: 20%.

The relative volume variation in the FCC-BCC transition in the Au-Fe alloy at $P = 0$ and $T = 300\,K$ is the same as the one in the $\gamma-\alpha$ transition in pure iron at $P = 0$ and $T = 1184\,K$ [9,31,32]. This suggests that iron is central to this transition in the alloy. However, the variations of parameters γ, z, B_T, $B'(P)$, α_p, $\alpha'_p(P)$, $C'_v(P)$, $C'_p(P)$, X_{sc}, μ_p, and $\sigma'(P)_T$ in this transition in the Au-Fe alloy are much greater than the corresponding variations in the $\gamma-\alpha$ transition in pure iron.

Table 4. Calculated properties of the FCC and BCC structures of the $Au_{1-C}Fe_C$ alloy at $C_f = 0.683$, $T = 300$ K, and $P = 0$

Property [unit of measurement]	fcc-Au-Fe	bcc-Au-Fe	$\Delta X \times 100$
$R = r_o/c$ — relative linear density	0.99600	0.99588	−0.012
$V = [\pi N/(6k_p)]c^3$ [cm^3/mol]	8.0169	8.10496	1.098
c [10^{-10} m]	2.6603	2.5955	−2.436
l — lattice parameter [10^{-10} m]	3.7622	2.9970	−20.339
Θ — Debye temperature [K]	340.063	340.506	0.130
$\gamma = -(\partial \ln \Theta/\partial \ln V)_T$ — Gruneisen parameter	2.1645	2.1521	−0.573
$q \cdot 10^3 = [(\partial \ln \gamma/\partial \ln V)_T] \cdot 10^3$	8.6904	8.6519	−0.443
$z = -(\partial \ln q/\partial \ln V)_T$	2.1817	2.1693	−0.568
$B_T = -\nu(\partial P/\partial \nu)_T$ — elastic modulus [GPa]	173.750	165.346	−4.837
$B'(P) = (\partial B_T/\partial P)_T^{1)}$	6.720	6.664	−0.833
$\alpha_p = \gamma C_v/(B_T V)$ [10^{-6} K^{-1}]	36.508	37.723	3.328
$\alpha_p \cdot B_T = (\partial P/\partial T)_v = (\partial s/\partial v)_T$ [10^{-3} GPa/K]	6.343	6.237	−1.671
$C_v/(Nk_B)$ — isochoric heat capacity	2.82565	2.82522	−0.015
$C_p/(Nk_B) = [C_v/(Nk_B)](1 + \gamma \alpha_p T)$	2.89264	2.89402	0.048
s/k_B — normalized specific entropy	3.57574	3.57206	−0.103
$\Theta'(P) = (\partial \Theta/\partial P)_T$ [K/GPa]$^{1)}$	4.2354	4.4327	4.658
$C'_v(P)/(Nk_B)$ [10^{-3}/GPa]$^{1)}$	−4.1782	−4.3911	5.095
$\alpha'_p(P) = (\partial \alpha_p/\partial P)_T$ [10^{-6}/(K·GPa)]$^{1)}$	−1.2573	−1.3525	7.572
$C'_p(P)/(Nk_B)$ [10^{-3}/GPa]$^{1)}$	−6.5877	−6.9689	5.787
$\sigma(100)$ — surface energy [10^{-3} J/m^2]	1955.30	1941.13	−0.725
$X_{sc} \cdot 10^3 = 10^3 \cdot \sigma(100)/(cB_T)$	42.302	45.232	6.926
μ_p — Poisson's ratio	0.3949	0.4006	1.443
$\sigma'(T)_v = (\partial \sigma/\partial T)_v$ [10^{-6} J/(m^{2}K)]	−57.650	−57.223	−0.741
$\sigma'(T)_P = (\partial \sigma/\partial T)_P$ [10^{-6} J/(m^{2}K)]	−108.168	−109.017	0.789
$\sigma'(P)_T = (\partial \sigma/\partial P)_T$ [10^{-3} J/(m^{2}GPa)]$^{1)}$	7.9617	8.3012	4.264
$\Delta_p = -(\partial \ln \sigma/\partial \ln \Sigma)_T = -0.5(\partial \ln \sigma/\partial \ln c)_T$	1.06156	1.06099	−0.054

N o t e. $^{1)}$ Calculated by differentiating the parameter numerically with respect to pressure along the isothermal dependence.
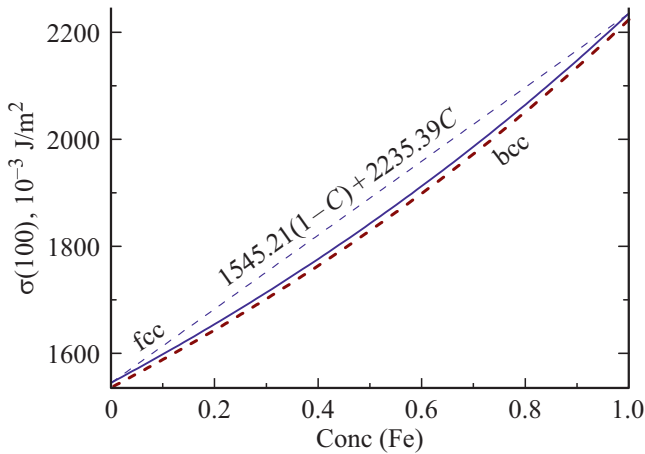
Figure 6. Concentration dependences of the specific surface energy of face (100) for the FCC (solid curve) and BCC (dashed curve) structures of the Au-Fe alloy. The dashed straight line represents the linear dependence of the arithmetic mean over the Fe concentration of the specific surface energies of pure FCC Au and Fe crystals.

vicinity of the FCC-BCC transition. This suggests that the Au-Fe alloy is prone to the metastable coexistence of the FCC and BCC structures in a wide range of concentrations
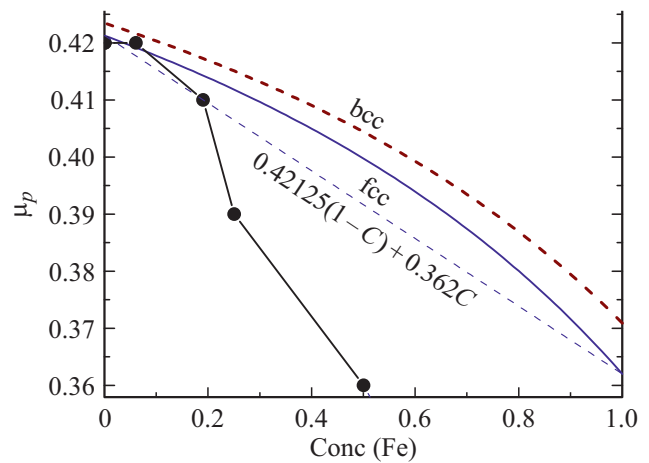
Figure 7. Concentration dependences of the Poisson's ratio for the FCC (solid curve) and BCC (dashed curve) structures of the Au-Fe alloy. Dots denote the results from [22] for FCC Au-Fe. The dashed straight line represents the linear dependence of the arithmetic mean over the Fe concentration of the Poisson's ratios of pure FCC Au and Fe crystals.

It can be seen from Fig. 1 that the energy difference between the FCC and BCC structures of the Au-Fe alloy remains very small in a wide range of concentrations in the

in the vicinity of the FCC-BCC transition. This is what accounts for the existence of the metastable X-ray amorphous structure in the $Au_{1-C}Fe_C$ alloy at $45 < C < 90\%$ [1,2,4].

The specific entropy decreases in the transition from the FCC structure to BCC in the Au-Fe alloy. This is indicative of absorption of the latent heat in this phase transition, which occurs in much the same way as in the $\gamma-\alpha$ transition in pure iron. At the same time, the relative variation of entropy in the FCC-BCC transition in the Au-Fe alloy is an order of magnitude smaller than the corresponding variation in the $\gamma-\alpha$ transition in pure iron:

$$\Delta s(\text{Au-Fe})/k_B = -0.00368,$$

$$\Delta s(\gamma-\alpha\text{-Fe})/k_B = -0.0746 \text{ [9]}, \quad -0.083 \text{ [31]}. \quad (8)$$

The small difference between the specific entropies of the FCC and BCC phases indicates that the Au-Fe alloy is prone to amorphization in the course of the FCC-BCC transition. Notably, it follows from (8) that the Au-Fe alloy is much more prone to amorphization in the FCC-BCC transition than pure Fe in the $\gamma-\alpha$ transition. The emergence of the X-ray amorphous state of pure Fe in the $\gamma-\alpha$ transition was observed experimentally in [32].

4. Variation of the parameters of the FCC-BCC c phase transition induced by a reduction in the size of nanoparticles of the Au-Fe alloy

The properties of a nanoparticle of the Au-Fe alloy with both FCC and BCC structures were calculated using the method from [6,7] and the parameters of interatomic potential (1) listed in Table 1. To preserve the axioms of equilibrium thermodynamics, we assumed that the alloy components are distributed evenly within the volume of a nanoparticle and that density and concentration gradients are lacking.

Table 5 presents the values of concentration C_f at which the thermodynamic potentials of the FCC and BCC phases of the $Au_{1-C}Fe_C$ alloy intersect in a macrocrystal ($N = \infty$, $k_n(\text{fcc}) = 12$, $k_n(\text{BCC}) = 8$) and a cubic nanoparticle with $N = 60000$ atoms. The average first coordination numbers for the FCC and BCC nanoparticle structures are

$$k_n(\text{fcc}) = 11.756617, \quad k_n(\text{BCC}) = 7.828296.$$

It follows from Table 5 that the value of C_f increases with an isochoric-isothermal reduction in the number of atoms in $Au_{1-C}Fe_C$ nanoparticles; i.e., the FCC-BCC transition shifts toward higher iron concentrations. If the number of atoms in a nanoparticle and the shape of its surface are fixed, the value of C_f increases with an isochoric increase in temperature and decreases with an isothermal reduction in density.

The results of calculations revealed that the thermodynamic potentials of the FCC and BCC phases of the

Table 5. Variation of concentration C_f (the concentration at which the FCC-BCC transition occurs in the $Au_{1-C}Fe_C$ alloy) with temperature and density for a macrocrystal and a nanocrystal of 60000 atoms

N	T, K	$R = r_o/c$	C_f
∞	10	1	0.680
	300	1	0.684
	300	0.9958	0.683
60000	10	1	0.970
	10	0.9958	0.969
	300	1	0.944
	300	0.9958	0.943

Au-Fe alloy at $P = 0$ and $T \leq 300$ K cease to intersect at $N < 59900$. In other words, the FCC structure of the Au-Fe alloy at $N < 59900$ (i.e., with nanoparticle diameter $d < 150 \cdot 10^{-10}$ m) is more stable than the BCC structure at any concentration of iron. At high iron concentrations ($C > 0.9$), relatively large ($40000 < N < 59900$) nanoparticles of the Au-Fe alloy may maintain a metastable amorphous structure with a mixture of FCC and BCC structures; however, the FCC structure becomes energetically favorable as nanoparticles decrease in size.

Note that the variation of the nanoparticle structure with size was observed experimentally for many single-component materials and alloys [33–36]. For example, it was found in [33] that the BCC structure of an iron nanoparticle changes to the FCC one, which is stable for macroscopic iron only at high temperatures, as the nanoparticle decreases in size. It was demonstrated experimentally in [34] that nanoparticles of the Au-Fe alloy cease to undergo the structural phase transition to the BCC phase below a certain size limit. It was also demonstrated experimentally in [35] that the high-temperature FCC phase of the Au-Fe alloy subjected to the FCC-BCC transition has a stable small size that is smaller than the one corresponding to the low-temperature BCC phase. The authors of review [36] noted the experimental studies where Au nanoparticles with stable crystal structures differing from the FCC structure were synthesized.

5. Conclusion

The parameters of the pairwise interatomic Mie–Lennard-Jones interaction potential for the FCC and BCC structures of gold and iron were determined in a self-consistent way. They were obtained by fitting the parameters of the potential for BCC gold to the point of intersection of the thermodynamic potentials at $T = 10$ K and $R = 1$ for the FCC and BCC phases of the disordered substitution $Au_{1-C}Fe_C$ alloy with iron concentration $C_f = 0.68$.

The determined parameters of interatomic potential (1) and the analytical method from [6,9] were used to calculate the properties of the FCC and BCC phases of gold and iron at $P = 0$ and $T = 300$ K. The results agreed well with experimental estimates, thus verifying the correctness of the calculation method.

The concentration dependences of the properties of the FCC and BCC phases of the Au-Fe alloy at $R = 1$ and $T = 300$ K were calculated. It was found that these dependences are nonlinear and agree with the results of calculations [22] for the FCC Au-Fe alloy performed using the density functional theory. The emergence of a metastable amorphous structure in a wide range of concentrations in the vicinity of the FCC-BCC transition in the Au-Fe alloy was explained.

The variation of the properties of the Au-Fe alloy in the structural FCC-BCC phase transition at $P = 0$ and $T = 300$ K was calculated. It was found that the values of R, Θ, γ, z, $B'(P)$, C_v, C_p, s, $\sigma(100)$, $\sigma'(T)_v$, $\sigma'(T)_P$, and Δ_p remain almost unchanged in the process of the FCC-BCC transition. The lattice parameter undergoes the greatest change, while the other examined properties vary within $1-7.6\%$. This pattern of parameter variation in the FCC-BCC transition allowed us to conclude that iron is central to the phase transition in the Au-Fe alloy.

The shift of concentration C_f, which corresponds to the intersection of the thermodynamic potentials of the FCC and BCC phases of the $Au_{1-C}Fe_C$ alloy, with a reduction in the nanoparticle size was calculated. It was demonstrated that the value of C_f shifts toward higher iron concentrations with an isochoric-isothermal reduction in the number of atoms in Au-Fe nanoparticles.

If the number of atoms in a nanoparticle and the shape of its surface are fixed, the value of C_f increases with an isochoric increase in temperature and decreases with an isothermal reduction in density. The calculations revealed that the FCC structure of a nanoparticle of the $Au_{1-C}Fe_C$ alloy at $P = 0$, $T \leq 300$ K, and $N < 59900$ is more stable than the BCC structure at any concentration of iron.

Conflict of interest

The author declares that he has no conflict of interest.

References

[1] H. Okamoto, T.B. Massalski, L.J. Swartzendruber, P.A. Beck. Bull. Alloy Phase Diagrams **5**, *6*, 592 (1984). DOI: 10.1007/BF02868322

[2] T.B. Massalski, H. Okamoto, P.R. Subramanian, L. Kacprzak. Binary Alloy Phase Diagrams (ASM, USA, 1992), V. 1-3.

[3] J.A. Munoz, M.S. Lucas, L. Mauger, I. Halevy, J. Horwath, S.L. Semiatin, Y. Xiao, P. Chow, M.B. Stone, D.L. Abernathy, B. Fultz. Phys. Rev. B **87**, *1*, 014301 (2013). DOI: 10.1103/PhysRevB.87.014301

[4] I.A. Zhuravlev, S.V. Barabash, J.M. An, K.D. Belashchenko. Phys. Rev. B **96**, *13*, 134109 (2017). DOI: 10.1103/PhysRevB.96.134109

[5] A. Tymoczko, M. Kamp, O. Prymak, C. Rehbock, J. Jakobi, U. Schürmann, L. Kienle, S. Barcikowski. Nanoscale **10**, *35*, 16434 (2018). DOI: 10.1039/c8nr03962c

[6] M.N. Magomedov. Phys. Solid State **62**, *12*, 2280 (2020). DOI: 10.1134/S1063783420120197

[7] M.N. Magomedov. Crystallography Rep. **62**, *3*, 480 (2017). DOI: 10.1134/S1063774517030142

[8] E.A. Moelwyn-Hughes. Phys. Chem. Pergamon Press, London (1961).

[9] M.N. Magomedov. Phys. Solid State **63**, *2*, 215 (2021). DOI: 10.1134/S1063783421020165

[10] M.N. Magomedov. Phys. Solid State **62**, *7*, 1126 (2020). DOI: 10.1134/S1063783420070136

[11] M.N. Magomedov. J. Surface Investigation. X-ray, Synchrotron Neutron Techniques **14**, *6*, 1208 (2020). DOI: 10.1134/S1027451020060105

[12] M.N. Magomedov. Technical Phys. **60**, *11*, 1619 (2015). DOI: 10.1134/S1063784215110195

[13] R. Briggs, F. Coppari, M.G. Gorman, R.F. Smith, S.J. Tracy, A.L. Coleman, A. Fernandez-Pa nella, M. Millot, J.H. Eggert, D.E. Fratanduono. Phys. Rev. Lett. **123**, *4*, 045701 (2019). DOI: 10.1103/PhysRevLett.123.045701

[14] S.S. Batsanov, A.S. Batsanov. Introduction to structural chemistry. Springer Science & Business Media, Heidelberg (2012). 545 p. DOI: 10.1007/978-94-007-4771-5

[15] M.N. Magomedov. Phys. Solid State **60**, *5*, 981 (2018). DOI: 10.1134/S1063783418050190

[16] M.N. Magomedov. Phys. Solid State **61**, *11*, 2145 (2019). DOI: 10.1134/S1063783419110210

[17] F. Calvo, N. Combe, J. Morillo, M. Benoit. J. Phys. Chem. C **121**, *8*, 4680 (2017). DOI: 10.1021/acs.jpcc.6b12551

[18] M.G. Pamato, I.G. Wood, D.P. Dobson, S.A. Hunt, L. Vočadlo. J. Appl. Crystallography **51**, *2*, 470 (2018). DOI: 10.1107/S1600576718002248

[19] M.M. Shukla, N.T. Padial. Rev. Brasil. Física **3**, *1*, 39 (1973). http://sbfisica.org.br/bjp/download/v03/v03a03.pdf

[20] V.K. Kumikov, Kh.B. Khokonov. J. Appl. Phys. **54**, *3*, 1346 (1983). DOI: 10.1063/1.332209

[21] A. Patra, J.E. Bates, J. Sun, J.P. Perdew. Proc. Nat. Acad. Sci. **114**, *44*, E9188-E9196 (2017). DOI: 10.1073/pnas.1713320114

[22] J. Kangsabanik, R.K. Chouhan, D.D. Johnson, A. Alam. Phys. Rev. B **96**, *10*, 100201 (2017). DOI: 10.1103/PhysRevB.96.100201

[23] P.I. Dorogokupets, A.M. Dymshits, K.D. Litasov, T.S. Sokolova. Sci. Rep. **7**, *41863*, 1 (2017). DOI: 10.1038/srep41863

[24] S.K. Saxena, G. Eriksson. J. Phys. Chem. Solids **84**, 70 (2015). DOI: 10.1016/j.jpcs.2015.03.006

[25] Y. Nishihara, Y. Nakajima, A. Akashi, N. Tsujino, E. Taka-hashi, K.I. Funakoshi, Y. Higo. Am. Mineralogist **97**, *8-9*, 1417 (2012). DOI: 10.2138/am.2012.3958

[26] H. Chamati, N.I. Papanicolaou, Y. Mishin, D.A. Papaconstan-topoulos. Surface Science **600**, *9*, 1793 (2006). DOI: 10.1016/j.susc.2006.02.010

[27] S.I. Novikova. Teplovoe rasshirenie tverdyh tel (Nauka, M., 1974), 294 p. (in Russian).

[28] S. Schönecker, X. Li, B. Johansson, S.K. Kwon, L. Vitos. Sci. Rep. **5**, 14860 (2015). DOI: 10.1038/srep14860

[29] D.J. Dever. J. Appl. Phys. **43**, *8*, 3293 (1972). DOI: 10.1063/1.1661710

[30] V.E. Zinov'ev. Teplofizicheskie svoista metallov pri vysokikh temperaturakh (The Thermophysical Proper ties of Metals at High Temperatures). Metallurgiya, Moscow (1989). 384 p.

[31] L.J. Swartzendruber. Bull. Alloy Phase Diagrams **3**, *2*, 161 (1982). DOI: 10.1007/BF02892374

[32] A.M. Balagurov, I.A. Bobrikov, I.S. Golovin. JETP Lett. **107** (9), 558 (2018). DOI: 10.7868/S0370274X18090084

[33] P.A. Montano, J. Zhao, M. Ramanathan, G.K. Shenoy, W. Schulze. In: Small Particles and Inorganic Clusters / Ed. C. Chapon, M.F. Gillet, C.R. Henry. Springer, Berlin, Heidelberg (1989). DOI: 10.1007/978-3-642-74913-1_23

[34] P. Mukherjee, X. Jiang, Y.Q. Wu, M.J. Kramer, J.E. Shield. J. Phys. Chem. C **117**, *45*, 24071 (2013). DOI: 10.1021/jp409015y

[35] D. Amram, C.A. Schuh. Phys. Rev. Lett. **121**, *14*, 145503 (2018). DOI: 10.1103/PhysRevLett.121.145503

[36] C. Sow, G. Mettela, G.U. Kulkarni. Annu. Rev. Mater. Res. **50**, 345 (2020). DOI: 10.1146/annurev-matsci-092519-103517